HYPERSPECTRAL IMAGE DENOISING VIA CONVEX LOW-FIBERED-RANK REGULARIZATION

Yu-Bang Zheng, Ting-Zhu Huang, Xi-Le Zhao*, Tai-Xiang Jiang, Jie Huang*

School of Mathematical Sciences/Research Center for Image and Vision Computing,
University of Electronic Science and Technology of China, Chengdu, Sichuan 611731, P.R.China

ABSTRACT

In this paper, we propose a new tensor rank, named fibered rank, by generalizing the tensor singular value decomposition (t-SVD) to the mode-k t-SVD. It factorizes a three-way tensor into two mode-k orthogonal tensors and a mode-k diagonal tensor. To efficiently remove mixed noise and finely preserve the structure information, we propose a novel hyperspectral image denoising model based on the three-directional tensor nuclear norm (3DTNN), which is a convex relaxation of the fibered rank. An efficient alternating direction method of multipliers (ADMM)-based algorithm is developed to solve the proposed model. Experimental results demonstrate the superiority of the proposed method over the compared ones.

***Index Terms*—** Hyperspectral image, fibered rank, tensor nuclear norm, alternating direction method of multipliers.

1. INTRODUCTION

Hyperspectral images (HSIs) contain wealthy spatial-spectral knowledge and have been widely used in many applications [1]. However, HSIs in real applications always suffer from various noises, such as Gaussian noise, sparse noise, and stripes. The noises preclude the widespread employ of HSIs for subsequent processing tasks, such as target detection and unmixing. Therefore, HSI denoising is an essential and critical preprocessing step for HSI applications [2–4]. The conclusive issue of HSI denoising is to explore rationally extract spatial-spectral prior knowledge of HSIs. Generally, the nonlocal self-similarity, the piecewise smoothness, and the low rankness are often taken into consideration.

The nonlocal self-similarity assumes that HSIs contain many similar cubes at different locations. This form of prior has been fully exploited in BM4D [5], which first searches similar 3D cubes and then removes noise collaboratively. The piecewise smoothness means that HSIs are local continuous along both spatial and spectral modes. To exploit this prior, Yuan et al. [6] designed a spectral-spatial adaptive total variation (SSAHTV); and Aggarwal and Majumdar [7] introduced the spatio-spectral total variation (SSTV). For low-rank prior, one classic work is the low-rank matrix recovery (LRMR)-based HSI denoising method [8].

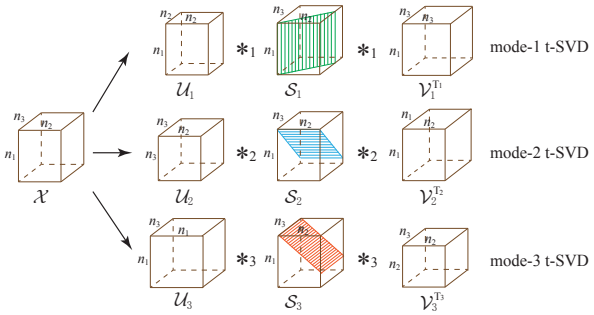

Fig. 1. Illustration of the mode-k t-SVD of $\mathcal{X}$ for $k = 1, 2, 3$.

Since an HSI can be regarded as a three-way tensor, many denoising methods are devoted to designing the tensor decomposition algorithms and the corresponding tensor ranks, such as the low-rank tensor approximation (LRTA) based on Tucker decomposition [9]. As the recent popular tensor tubal rank, defined based on the tensor singular value decomposition (t-SVD), obtains promising results [10], Fan et al. [11] proposed an HSI denoising model via low-tubal-rank tensor recovery (LRTR). However, within the framework of t-SVD, for a three-way tensor, the correlations along the first and the second modes are characterized by the SVD while the correlation along the third mode is encoded by the embedded circular convolution. It means that t-SVD and tubal rank lack direct characterization for the correlation along spectral mode.

Contributions. (1) We propose a new definition for tensor rank, termed as tensor fibered rank, by generalizing the t-SVD to the mode-k t-SVD (See Fig. 1). (2) To efficiently remove mixed noise, we propose a novel HSI denoising model based on the three-directional tensor nuclear norm (3DTNN), a convex relaxation of the fibered rank. An efficient alternating direction method of multipliers (ADMM)-based algorithm is developed to solve the proposed model.

The outline of this paper is as follows. Section 2 presents some notations. Section 3 defines the fibered rank and its relaxation 3DTNN. Section 4 proposes a 3DTNN-based HSI denoising model with an ADMM-based solver. Section 5 evaluates the performance of the proposed model. Section 6 concludes this paper.

This work is supported by NSFC (61772003, 61876203) and the Fundamental Research Funds for the Central Universities (ZYGX2016J132).
*Corresponding authors:tingzhuhuang@126.com;xlzhao122003@163.com.

2. NOTATIONS

For $\mathcal{X} \in \mathbb{R}^{n_1 \times n_2 \times n_3}$, we use $X_1^{(i_1)} \in \mathbb{R}^{n_2 \times n_3}$, $X_2^{(i_2)} \in \mathbb{R}^{n_3 \times n_1}$, and $X_3^{(i_3)} \in \mathbb{R}^{n_1 \times n_2}$ to denote its i_1-th mode-1 (horizontal), i_2-th mode-2 (lateral), and i_3-th mode-3 (frontal) slices, respectively. We use $\bar{\mathcal{X}}_k$ to denote the tensor generated by performing the Discrete Fourier Transformation (DFT) along each mode-k fiber of $\mathcal{X}$, i.e., $\bar{\mathcal{X}}_k = \texttt{fft}(\mathcal{X}, [], k)$.

3. THE FIBERED RANK AND ITS RELAXATION

In this section, we design the mode-k t-SVD, and propose the tensor fibered rank and its convex relaxation 3DTNN.

We define the following mode-k t-product, which can be regarded as a matrix-matrix multiplication, except that the multiplication operation between scalars is replaced by circular convolution between the mode-k fibers.

Definition 1 (mode-k t-product) The mode-k t-product $(*_k)$ between two three-way tensors $\mathcal{X}$ and $\mathcal{Y}$ is defined as

$$\mathcal{F} = \mathcal{X} *_1 \mathcal{Y} \Leftrightarrow \mathcal{F}(:,j,s) = \sum_{t=1}^{n_3} \mathcal{X}(:,j,t) \star \mathcal{Y}(:,t,s),$$
$$\mathcal{F} = \mathcal{X} *_2 \mathcal{Y} \Leftrightarrow \mathcal{F}(i,:,s) = \sum_{t=1}^{n_1} \mathcal{X}(t,:,s) \star \mathcal{Y}(i,:,t),$$
$$\mathcal{F} = \mathcal{X} *_3 \mathcal{Y} \Leftrightarrow \mathcal{F}(i,j,:) = \sum_{t=1}^{n_2} \mathcal{X}(i,t,:) \star \mathcal{Y}(t,j,:),$$

where $\star$ denotes the circular convolution and $\mathcal{X} \in \mathbb{R}^{n_1 \times n_2 \times n_3}$.

Next, we define the mode-k conjugate transpose and some special tensors.

Definition 2 (mode-k conjugate transpose) The mode-k conjugate transpose of a three-way tensor $\mathcal{X} \in \mathbb{R}^{n_1 \times n_2 \times n_3}$, denote as $\mathcal{X}^{\mathrm{T}_k}$, is the tensor obtained by conjugate transposing each of the mode-k slices and then reversing the order of transposed mode-k slices 2 through n_k.

Definition 3 (some special tensors) The mode-k identity tensor $\mathcal{I}_k$ is the tensor whose first mode-k slice is the identity matrix, and other mode-k slices are all zeros.

A three-way tensor $\mathcal{Q}$ is mode-k orthogonal if $\mathcal{Q} *_k \mathcal{Q}^{\mathrm{T}_k} = \mathcal{Q}^{\mathrm{T}_k} *_k \mathcal{Q} = \mathcal{I}_k$.

A three-way tensor $\mathcal{S}$ is mode-k diagonal if each of its mode-k slices is a diagonal matrix.

With the above definitions, we design the mode-k t-SVD.

Theorem 1 (mode-k t-SVD) Assuming that $\mathcal{X} \in \mathbb{R}^{n_1 \times n_2 \times n_3}$ is a three-way tensor, then it can be factored as

$$\mathcal{X} = \mathcal{U}_k *_k \mathcal{S}_k *_k \mathcal{V}_k^{\mathrm{T}_k}, \ k = 1, 2, 3,$$

where $\mathcal{U}_k$ and $\mathcal{V}_k$ are the mode-k orthogonal tensors, and $\mathcal{S}_k$ is the mode-k diagonal tensor.

Since the circular convolution in the spatial domain is equivalent to the multiplication in the Fourier domain, the mode-k t-SVD can be efficiently obtained by computing a series of matrix SVDs in the Fourier domain.

Definition 4 (mode-k fibered rank and mode-k multi rank) For a three-way tensor $\mathcal{X} \in \mathbb{R}^{n_1 \times n_2 \times n_3}$, the mode-$k$ fibered rank of it, denoted as $\mathrm{rank}_{\mathrm{f}_k}(\mathcal{X})$, is defined as the number of non-zero mode-k fibers of $\mathcal{S}_k$, where $\mathcal{S}_k$ comes from the mode-k t-SVD of $\mathcal{X}$. The mode-k multi rank of $\mathcal{X}$ is a vector $\mathrm{rank}_{\mathrm{m}_k}(\mathcal{X}) \in \mathbb{R}^{n_k}$, whose i-th element is the rank of i-th mode-k slice of $\bar{\mathcal{X}}_k$, where $\bar{\mathcal{X}}_k = \texttt{fft}(\mathcal{X}, [], k)$. That is, $\mathrm{rank}_{\mathrm{f}_k}(\mathcal{X}) = \max\left(\mathrm{rank}_{\mathrm{m}_k}(\mathcal{X})\right)$.

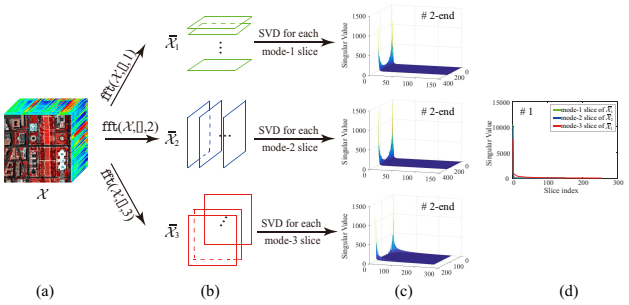

Fig. 2. Illustration of low-fibered-rank property of an HSI. (a) The HSI *Washington DC Mall* of size $256 \times 256 \times 150$. (b) The tensor $\bar{\mathcal{X}}_k$ generated by performing the DFT along each mode-k fiber of $\mathcal{X}$. (c) Singular value curves from the second to the end mode-k slices of $\bar{\mathcal{X}}_k$. (d) Singular value curves of the first mode-k slices of $\bar{\mathcal{X}}_k$.

Table 1. The rank estimation of an HSI.

Data	Size	Tucker rank	Tubal rank	Fibered rank
Washington DC Mall	256× 256×150	(107,110,6)	182	(8,8,182)

Actually, the tensor tubal/multi rank is actually the mode-3 fibered/multi rank. We define the following tensor fibered rank to combine all mode-k ($k = 1, 2, 3$) fibered rank.

Definition 5 (tensor fibered rank) The fibered rank of a three-way tensor $\mathcal{X}$, denoted as $\mathrm{rank}_{\mathrm{f}}(\mathcal{X})$, is defined as a vector, whose k-th element is the mode-k fibered rank.

Table 1 gives the rank estimation of the HSI *Washington DC Mall*[1] and Fig. 2 visually shows its low-fibered-rank property. As observed, the proposed fibered rank has the advantage of simultaneous characterization for the correlations along different modes. As minimizing the fibered rank is NP-hard, we propose the 3DTNN as its convex relaxation.

Definition 6 (mode-k TNN) The mode-k tensor nuclear norm of a tensor $\mathcal{X} \in \mathbb{R}^{n_1 \times n_2 \times n_3}$, denoted as $\|\mathcal{X}\|_{\mathrm{TNN}_k}$, is defined as the sum of singular values of all the mode-k slices of $\bar{\mathcal{X}}_k$, i.e., $\|\mathcal{X}\|_{\mathrm{TNN}_k} := \sum_{i=1}^{n_k} \left\|(\bar{X}_k)_k^{(i)}\right\|_*$, where $(\bar{X}_k)_k^{(i)}$ is the i-th mode-k slice of $\bar{\mathcal{X}}_k$.

Definition 7 (3DTNN) The three-directional nuclear norm of a tensor $\mathcal{X} \in \mathbb{R}^{n_1 \times n_2 \times n_3}$, denoted as $\|\mathcal{X}\|_{\mathrm{3DTNN}}$, is defined as a weighted sum of all the mode-k tensor nuclear norms of $\mathcal{X}$, i.e., $\|\mathcal{X}\|_{\mathrm{3DTNN}} := \sum_{k=1}^{3} \alpha_k \|\mathcal{X}\|_{\mathrm{TNN}_k}$, where $\alpha_k \geq 0$ $(k = 1, 2, 3)$ and $\sum_{k=1}^{3} \alpha_k = 1$.

TNN has shown its effectiveness to preserve the intrinsic structure of the three-way tensors [10]. Therefore, as the weighted sum of all the mode-k TNN, the proposed 3DTNN can effectively exploit the correlations along all modes while preserving the intrinsic structure of the underlying tensor. Especially, we can easily prove that the 3DTNN is numerically equal to the triple tubal nuclear norm proposed in [12].

[1] http://lesun.weebly.com/hyperspectral-data-set.html

Algorithm 1 ADMM-based optimization algorithm for the 3DTNN-based HSI denosing model.

Input: The noisy HSI $\mathcal{Y}$, parameters $\alpha = (\alpha_1, \alpha_2, \alpha_3)$, $\mu = (\mu_1, \mu_2, \mu_3)$, λ_1, λ_2, β and $\rho = 1.2$.

Initialization: $p = 0$, $\mathcal{X}^0 = 0, \mathcal{N}^0 = 0, \mathcal{S}^0 = 0$, $\mathcal{Z}_k^0 = 0$, $\mathcal{M}_k^0 = 0$, and $\mathcal{P}^0 = 0$.

1: **while** not converged **do**

2: Update $\mathcal{Z}_k^{p+1} = \mathcal{D}_{\alpha_k/\mu_k}(\mathcal{X}^p + \mathcal{M}_k^p/\mu_k, k)$, $k = 1, 2, 3$.

3: Update $\mathcal{X}^{p+1} = \big(\sum_{k=1}^3(\mu_k\mathcal{Z}_k^{p+1} - \mathcal{M}_k^p) + (\beta\mathcal{Y} - \beta\mathcal{N}^p - \beta\mathcal{S}^p + \mathcal{P}^p)\big)/(\sum_{k=1}^3\mu_k + \beta)$.

4: Update $\mathcal{N}^{p+1} = \big(\beta\mathcal{Y} - \beta\mathcal{X}^{p+1} - \beta\mathcal{S}^p + \mathcal{P}^p\big)/(2\lambda_1 + \beta)$.

5: Update $\mathcal{S}^{p+1} = \texttt{shrink}\big(\mathcal{Y} - \mathcal{X}^{p+1} - \mathcal{N}^{p+1} + \frac{\mathcal{P}^p}{\beta}, \frac{\lambda_2}{\beta}\big)$, where $\big[\texttt{shrink}(\mathcal{X}, \xi)\big]_{ijs} = \text{sgn}(x_{ijs})\max(|x_{ijs}| - \xi, 0)$.

6: Update $\mathcal{M}_k^{p+1} = \mathcal{M}_k^p + \mu_k(\mathcal{X}^{p+1} - \mathcal{Z}_k^{p+1})$, $k = 1, 2, 3$; $\mathcal{P}^{p+1} = \mathcal{P}^p + \beta\big(\mathcal{Y} - (\mathcal{X}_k^{p+1} + \mathcal{N}_k^{p+1} + \mathcal{S}_k^{p+1})\big)$.

7: Let $\mu = \rho\mu$; $\beta = \rho\beta$; $p = p + 1$.

8: Check the convergence condition $\|\mathcal{X}^{(p+1)} - \mathcal{X}^{(p)}\|_F / \|\mathcal{X}^{(p)}\|_F < 10^{-4}$.

9: **end while**

Output: The restored HSI $\mathcal{X}$.

4. THE 3DTNN-BASED HSI DENOISING MODEL

Considering a three-way tensor $\mathcal{X} \in \mathbb{R}^{n_1\times n_2\times n_3}$, the proposed 3DTNN-based HSI denoising model is formulated as

$$\begin{aligned} \min_{\mathcal{X},\mathcal{N},\mathcal{S}} \ & \|\mathcal{X}\|_{\text{3DTNN}} + \lambda_1\|\mathcal{N}\|_F^2 + \lambda_2\|\mathcal{S}\|_1, \\ \text{s.t.} \ & \mathcal{Y} = \mathcal{X} + \mathcal{N} + \mathcal{S}, \end{aligned} \tag{1}$$

where $\mathcal{X}$ is the underlying HSI, $\mathcal{Y}$ is the observed HSI, $\mathcal{N}$ is the Gaussian noise, $\mathcal{S}$ is the sparse noise, and λ_1 and λ_2 are the tuning parameters. The problem (1) can be rewritten as

$$\begin{aligned} \min_{\mathcal{X},\mathcal{N},\mathcal{S}} \ & \sum_{k=1}^3 \alpha_k\|\mathcal{X}\|_{\text{TNN}_k} + \lambda_1\|\mathcal{N}\|_F^2 + \lambda_2\|\mathcal{S}\|_1, \\ \text{s.t.} \ & \mathcal{Y} = \mathcal{X} + \mathcal{N} + \mathcal{S}, \end{aligned} \tag{2}$$

where $\alpha_k \geq 0$ $(k = 1, 2, 3)$ and $\sum_{k=1}^3 \alpha_k = 1$.

Next, we use the ADMM to solve (2). We introduce three auxiliary tensors $\mathcal{Z}_k$ $(k = 1, 2, 3)$ and reformulate (2) as

$$\begin{aligned} \min_{\mathcal{X},\mathcal{N},\mathcal{S},\mathcal{Z}_k} \ & \sum_{k=1}^3 \alpha_k\|\mathcal{Z}_k\|_{\text{TNN}_k} + \lambda_1\|\mathcal{N}\|_F^2 + \lambda_2\|\mathcal{S}\|_1, \\ \text{s.t.} \ & \mathcal{Y} - (\mathcal{X} + \mathcal{N} + \mathcal{S}) = 0, \\ & \mathcal{X} - \mathcal{Z}_k = 0, \ k = 1, 2, 3. \end{aligned} \tag{3}$$

The augmented Lagrangian function of (3) is

$$\begin{aligned} L_{\mu_k,\beta}(\mathcal{Z}_k, \mathcal{X}, \mathcal{N}, \mathcal{S}, \mathcal{M}_k, \mathcal{P}) &= \sum_{k=1}^3 \Big\{\alpha_k\big\|\mathcal{Z}_k\big\|_{\text{TNN}_k} \\ &+ \langle\mathcal{X} - \mathcal{Z}_k, \mathcal{M}_k\rangle + \mu_k/2\big\|\mathcal{X} - \mathcal{Z}_k\big\|_F^2\Big\} + \lambda_1\|\mathcal{N}\|_F^2 + \lambda_2\|\mathcal{S}\|_1 \\ &+ \langle\mathcal{Y} - (\mathcal{X} + \mathcal{N} + \mathcal{S}), \mathcal{P}\rangle + \beta/2\big\|\mathcal{Y} - (\mathcal{X} + \mathcal{N} + \mathcal{S})\big\|_F^2, \end{aligned}$$

where $\mathcal{M}_k$ $(k = 1, 2, 3)$, $\mathcal{P}$ are the Lagrange multipliers; μ_k $(k = 1, 2, 3)$ and β are the penalty parameters. Within the framework of ADMM, $\mathcal{Z}_k$, $\mathcal{X}$, $\mathcal{N}$, and $\mathcal{S}$ are alternately updated as shown in Algorithm 1. Particularly, the solution of $\mathcal{Z}_k$-subproblem is given by the following theorem.

Theorem 2 For a tensor $\mathcal{Z} \in \mathbb{R}^{n_1\times n_2\times n_3}$, a minimizer to

$$\arg\min_{\mathcal{Z}} \tau\|\mathcal{Z}\|_{\text{TNN}_k} + 1/2\|\mathcal{Z} - \mathcal{Y}\|_F^2,$$

is given by the tensor singular value thresholding operation $\mathcal{Z} = \mathcal{D}_\tau(\mathcal{Y}, k) := \mathcal{U}_k *_k \mathcal{S}_k^\tau *_k \mathcal{V}_k^{\text{T}_k}$, where $\mathcal{Y} = \mathcal{U}_k *_k \mathcal{S}_k *_k \mathcal{V}_k^{\text{T}_k}$ and $\bar{\mathcal{S}}_k^\tau = \max(\bar{\mathcal{S}}_k - \tau, 0)$.

The computational cost at each iteration of the proposed algorithm is $\mathcal{O}\big(n_1n_2n_3\big(\log(n_1n_2n_3) + \sum_{i=1}^3 \min(n_i, n_{i+1})\big)\big)$, where $n_4 = n_1$. The convergence of the developed algorithm within the ADMM framework is guaranteed theoretically, considering the convexity of the objective function.

5. NUMERICAL EXPERIMENTS

In this section, we evaluate the performance of the proposed 3DTNN-based HSI denoising method on the HSI *Washington DC Mall*, which is of size 256×256×191 and normalized to [0,1]. We employ the peak signal to noise rate (PSNR), the structural similarity (SSIM), and the spectral angle mapping (SAM) to measure the quality of the recovered results. The comparison methods include: TRPCA+BM4D [5, 13], SSTV [7], LRMR [8], and LRTR [11]. TRPCA+BM4D is a hybrid denoising method which first uses TRPCA to filter the sparse noise and then performs BM4D to remove Gaussian noise. The parameters of all compared methods are set based on authors' codes or suggestions in their papers. The noisy datasets are generated as follows.

Case 1: Synthetic data with different Gaussian noise, fixed salt and pepper noise, and fixed stripe noise. The zero-mean Gaussian noise is added to all bands and standard deviation σ are set to be 0.02, 0.06, and 0.10. The salt and pepper noise is added to all bands and the proportion υ is 0.2. Stripes are added to 10 bands from band 131 to 140. In each band, the percent of stripes is 10%.

Case 2: Synthetic data with different salt and pepper noise, fixed Gaussian noise, and fixed stripe noise. The salt and pepper noise is added to all bands and the proportion υ are set to be 0.1, 0.3 and 0.4. The zero-mean Gaussian noise is added to all bands and standard deviation σ is 0.02. Stripes are added to 10 bands from band 131 to 140. In each band, the percent of stripes is 10%.

Table 2 lists the PSNR, SSIM, SAM, and average running time (in seconds) of the testing HSI recovered by five competing methods. It can be observed that the proposed method consistently outperforms the compared methods in terms of PSNR, SSIM, and SAM values. In Fig. 3, we visually show the denoising results in one case. As observed,

Table 2. The performance comparison of five competing methods with respect to different noise levels.

Case	Case 1									Case 2									
Gaussian noise	$\sigma = 0.02$			$\sigma = 0.06$			$\sigma = 0.10$			$\sigma = 0.02$									average
Salt and pepper noise	$\upsilon = 0.2$									$\upsilon = 0.1$			$\upsilon = 0.3$			$\upsilon = 0.4$			time (s)
Method	PSNR	SSIM	SAM	PSNR	SSIM	SAM	PSNR	SSIM	SAM	PSNR	SSIM	SAM	PSNR	SSIM	SAM	PSNR	SSIM	SAM	
Noise	11.373	0.1212	47.389	11.188	0.1137	48.025	10.839	0.1023	49.172	14.357	0.2531	41.766	9.6182	0.0718	49.704	8.3756	0.0470	50.771	–
TRPCA+BM4D	38.798	0.9790	3.7193	33.657	0.9342	5.8150	30.991	0.8821	7.3463	39.900	0.9832	3.2894	37.273	0.9708	4.4344	33.336	0.9240	7.0538	973.81
SSTV	39.043	0.9754	4.3674	34.377	0.9326	6.6053	31.251	0.8734	8.8027	40.239	0.9804	4.0178	37.839	0.9682	4.8038	36.336	0.9562	5.4216	595.87
LRMR	35.196	0.9488	5.6839	33.653	0.9301	6.8313	31.516	0.8952	8.6890	38.597	0.9730	3.8940	32.704	0.9189	7.4550	30.588	0.8819	9.2499	73.816
LRTR	36.479	0.9629	5.1349	33.928	0.9331	6.2357	30.968	0.8923	8.4193	38.663	0.9741	3.7062	34.617	0.9428	6.2333	31.113	0.8717	9.2404	135.69
3DTNN	**41.658**	**0.9920**	**1.8010**	**35.554**	**0.9655**	**3.9101**	**32.398**	**0.9317**	**5.5411**	**42.794**	**0.9937**	**1.6046**	**40.345**	**0.9897**	**2.0145**	**38.629**	**0.9856**	**2.3506**	316.43

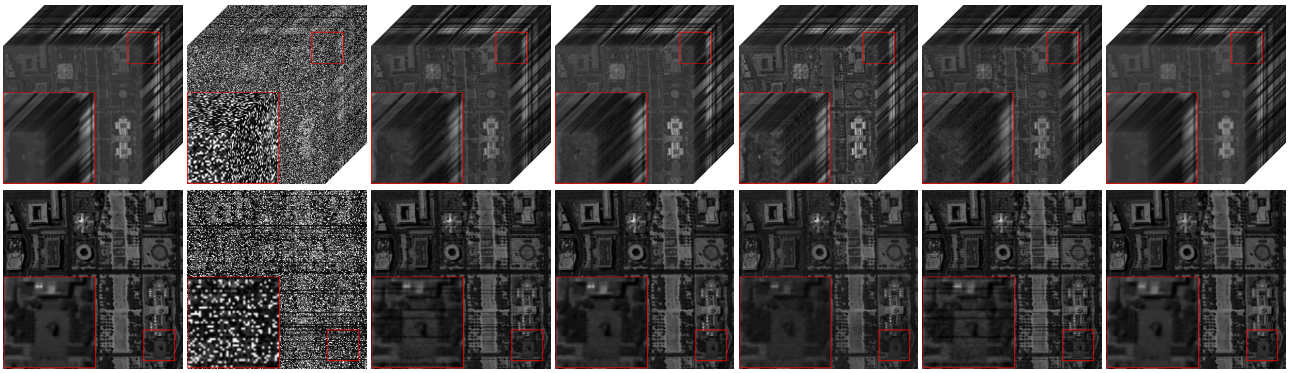

Fig. 3. The denoising results for the Gaussian noise with $\sigma = 0.02$ and the salt and pepper noise with $\upsilon = 0.4$. Top row: The three dimensional visualization of the denoising results. Bottom row: The denoising results at band 131.

the proposed method produces visually superior results than the compared methods. Specifically, the proposed method is capable of better removing the unexpected mixed noise while finely preserving the structure of the underlying HSI, while the results obtained by TRPCA+BM4D and LRTR remain a small amount of stripes. SSTV and LRMR can perform comparatively better in stripes removing, but their results remain a small amount of Gaussian noise or salt and pepper noise.

6. CONCLUSION

In this paper, we extended the t-SVD to mode-k t-SVD to depict the correlations along different modes, and then defined the tensor fibered rank and its convex relaxation 3DTNN. And we proposed a 3DTNN-based HSI denoising model and developed an efficient ADMM-based algorithm to solve it. Numerical results demonstrated the superiority of the proposed method in comparison with other state-of-the-art methods.

REFERENCES

[1] J. M. Bioucas-Dias, A. Plaza, N. Dobigeon, M. Parente, Q. Du, P. Gader, and J. Chanussot, "Hyperspectral unmixing overview: Geometrical, statistical, and sparse regression-based approaches," *IEEE Journal of Selected Topics in Applied Earth Observations and Remote Sensing*, vol. 5, no. 2, pp. 354–379, 2012.

[2] L. Zhuang and J. M. Bioucas-Dias, "Fast hyperspectral image denoising and inpainting based on low-rank and sparse representations," *IEEE Journal of Selected Topics in Applied Earth Observations and Remote Sensing*, vol. 11, no. 3, pp. 730–742, 2018.

[3] T.-X. Jiang, L. Zhuang, T.-Z. Huang, and J. M. Bioucas-Dias, "Adaptive hyperspectral mixed noise removal," in *IGARSS*, 2018, pp. 4035–4038.

[4] S. Li, R. Dian, L. Fang, and J. M. Bioucas-Dias, "Fusing hyperspectral and multispectral images via coupled sparse tensor factorization," *IEEE Transactions on Image Processing*, vol. 27, no. 8, pp. 4118–4130, 2018.

[5] M. Maggioni, G. Boracchi, A. Foi, and K. Egiazarian, "Video denoising, deblocking, and enhancement through separable 4-D nonlocal spatiotemporal transforms," *IEEE Transactions on Image Processing*, vol. 21, no. 9, pp. 3952–3966, 2012.

[6] Q. Yuan, L. Zhang, and H. Shen, "Hyperspectral image denoising employing a spectral-spatial adaptive total variation model," *IEEE Transactions on Geoscience and Remote Sensing*, vol. 50, no. 10, pp. 3660–3677, 2012.

[7] H. K. Aggarwal and A. Majumdar, "Hyperspectral image denoising using spatio-spectral total variation," *IEEE Geoscience and Remote Sensing Letters*, vol. 13, no. 3, pp. 442–446, 2016.

[8] H. Zhang, W. He, L. Zhang, H. Shen, and Q. Yuan, "Hyperspectral image restoration using low-rank matrix recovery," *IEEE Transactions on Geoscience and Remote Sensing*, vol. 52, no. 8, pp. 4729–4743, 2014.

[9] N. Renard, S. Bourennane, and J. Blanc-Talon, "Denoising and dimensionality reduction using multilinear tools for hyperspectral images," *IEEE Geoscience and Remote Sensing Letters*, vol. 5, no. 2, pp. 138–142, 2008.

[10] Z. Zhang and S. Aeron, "Exact tensor completion using t-SVD," *IEEE Transactions on Signal Processing*, vol. 65, no. 6, pp. 1511–1526, 2017.

[11] H. Fan, Y. Chen, Y. Guo, H. Zhang, and G. Kuang, "Hyperspectral image restoration using low-rank tensor recovery," *IEEE Journal of Selected Topics in Applied Earth Observations and Remote Sensing*, vol. 10, no. 10, pp. 4589–4604, 2017.

[12] D. Wei, A. Wang, X. Feng, B. Wang, and B. Wang, "Tensor completion based on triple tubal nuclear norm," *Algorithms*, vol. 11, no. 7, p. 94, 2018.

[13] C. Lu, J. Feng, Y. Chen, W. Liu, Z. Lin, and S. Yan, "Tensor robust principal component analysis: Exact recovery of corrupted low-rank tensors via convex optimization," in *CVPR*, 2016, pp. 5249–5257.